Hindawi
Advances in Materials Science and Engineering
Volume 2019, Article ID 5190235, 7 pages
https://doi.org/10.1155/2019/5190235

Research Article

Oxide Nanomaterials Based on SnO_2 for Semiconductor Hydrogen Sensors

George Fedorenko, Ludmila Oleksenko, and Nelly Maksymovych

Taras Shevchenko National University of Kyiv, 62a Volodymyrska Str., Kyiv 01601, Ukraine

Correspondence should be addressed to George Fedorenko; georgf@ukr.net

Received 11 April 2019; Accepted 18 July 2019; Published 5 August 2019

Guest Editor: Arslan Shehzad

Nanosized tin dioxide with an average particle size of 5.3 nm was synthesized by a sol-gel method and characterized by IR spectroscopy, TEM, X-ray, and electron diffraction. The obtained SnO_2 can be used as initial material for creation of gas-sensitive layers of adsorption semiconductor sensors. Addition of palladium into the initial nanomaterial allows to improve response to hydrogen of such sensors in comparison with sensors based on undoped SnO_2 and provides fast response and recovery time, a wide measuring range of hydrogen content in air ambient, and good repeatability of the sensor signal. Such promising properties could make useful the sensors based on these nanomaterials for devices intended to determine hydrogen in air.

1. Introduction

Nowadays, development of nanosized oxides is actual for obtaining functional materials with required properties. In particular, such nanomaterials can be useful for creating adsorption semiconductor gas sensors intended to determine the presence of combustible gases, e.g., hydrogen, in air. Different semiconductor oxides, such as SnO_2, TiO_2, ZnO, ZrO_2, and WO_3 [1–5], can be used as initial materials for gas-sensitive layers of the sensors. Tin dioxide among them is the most popular due to its chemical stability, band structure, and extreme sensitivity of its conductivity to the surface state where the molecules adsorbed on the SnO_2 surface are actively engaged in chemical reactions occurred in the temperature range 20–500°C [6–11]. It is known that a decrease in the particle size of semiconductor material can lead to increase in the ratio of the atoms fraction on the surface of particles to the atoms fraction in their volume that makes impact of the surface processes into the material properties significant [12]. Thus, the sensitivity of the adsorption semiconductor sensors should depend greatly on the morphology of the materials of the gas-sensitive layers: a decrease in the semiconductor particle size of the gas-sensitive material could cause an increase in the sensor response as it was experimentally observed by other authors [13–16].

Increase in the sensor response can also be achieved by introducing catalytically active additives into the semiconductor materials of the gas-sensitive layers [13]. It leads to an increase in the rate of the catalytic reaction of the analyzed gas with oxygen chemisorbed on the sensor surface that in turn increases the sensor response [13]. Palladium can be such an additive for hydrogen sensors due to its high catalytic activity in the hydrogen oxidation reaction [17].

Thus, usage of tin dioxide nanomaterial doped with the palladium additive is promising to provide high sensitivities of the semiconductor sensors to hydrogen.

The aim of this work is to synthesize oxide nanomaterials based on tin dioxide with the addition of palladium for creation of highly sensitive adsorption semiconductor sensors to hydrogen.

2. Experimental

Initial nanosized tin dioxide was synthesized by a sol-gel process through chemical oxidation of tin (II) oxalate by 35% solution of H_2O_2 [18]. Tin (II) oxalate (3 g) was gradually added under stirring to 10 ml of 35% solution of hydrogen peroxide in water. After two hours, a resulting sol was quickly heated to decompose the excess of the hydrogen peroxide and evaporate the water. As a result, a transparent

water-based gel was obtained, and then it was dried at 90°C for 24 hours until the gel turned into a yellowish translucent xerogel [19]. The xerogel was calcinated at different temperatures and temperature holding times for obtaining crystalline nanoscale SnO_2 particles with minimal sizes.

In order to optimize the temperature treatment conditions of the obtained xerogel, its thermal decomposition was studied in air with a heating rate of 10°C/min on a DTG-60H derivatograph (Shimadzu, Japan).

Gas-sensitive nanomaterials based on unmodified SnO_2 and tin dioxide doped with 0.24 wt.% palladium were obtained through applying a paste formed by mixing the initial nanosized SnO_2 with aqueous solution of carboxymethylcellulose (CMC) onto ceramic plates with subsequent drying at 90°C. Impregnation of the dried paste with a solution of palladium (II) chloride in dilute hydrochloric acid was performed with subsequent drying at 90°C in order to obtain palladium-doped gas-sensitive material. The coated ceramic plates were then heated at temperatures up to 620°C in order to provide decomposition of $PdCl_2$ and CMC.

The amount of palladium introduced into the gas-sensitive material was determined by X-ray fluorescence analysis (ElvaX EXS–01, Elvatech, Ukraine).

The morphology of the synthesized nanomaterial was studied by transmission electron microscopy on a SELMI PEM-125K device (Ukraine) with an accelerating voltage of 100 kV.

The phase composition of the materials was studied using a LabX XRD-6000 diffractometer, Shimadzu (Japan) (CuKα radiation). Particle sizes of the nanomaterials were estimated using the Scherrer equation [20]:

$$D = \frac{k\lambda}{\beta \cdot \cos\theta}, \quad (1)$$

where D is XRD particle size; k is a constant that depends on crystallite shape and is close to unity (for our calculation k was equal to 0.9); λ is the wavelength of CuKα radiation ($\lambda = 1{,}5418$ Å); β is a true broadening of diffraction peak ($\beta = \Delta - b$, where Δ is an experimental broadening of the diffraction peak; b is an instrumental broadening); and θ is a Bragg angle. The lattice parameters of the materials were calculated using a program UnitCell.

The specific surface areas of the xerogel temperature treatment products were determined by the argon thermal desorption method using Al_2O_3 as a standard sample ($S_{sp} = 22\ m^2/g$). Before measurements, the investigated samples were degassed in a helium stream at 300–350°C for two hours.

The infrared spectra of the samples were recorded on a PerkinElmer BX spectrophotometer (USA).

The sensors were made on the basis of planar ceramic plates by the same preparation method as the gas-sensitive nanomaterials. The paste (mixture of the initial nanosized SnO_2 with the 3% solution of CMC in water) was deposited between measuring electrodes on the one side of the ceramic sensor plate. The other side of the plate contained a platinum heater for controlling the operational temperature of the sensor. Dimensions of the sensors plates were $1.8 \times 1.8 \times 0.3$ mm. Design of the sensor in more detail is presented in [21].

The sensor parameters were determined in a special electric stand. The electrical circuit of the stand was presented in [22]. A hydrogen-air mixture with 44 ppm H_2 was used to measure the sensor responses at different operational temperatures in order to find optimal hydrogen sensing conditions.

Stabilization of the sensor electrical conductivities was achieved by pretreatment of the sensors for three days at the operational temperature of 405°C with a periodic supply of the hydrogen-air mixture (935 ppm H_2) to the measuring chambers where the sensors were placed.

The ratio of the sensor electrical conductivity in hydrogen-air mixture (σ_g) to the electrical conductivity in clean air (σ_0) was taken as a measure of the sensor response to this hydrogen content in air ambient (γ): $\gamma = \sigma_g/\sigma_0$.

Two parameters (response time ($\tau_{0.9}$) and recovery time (τ_{relax})) were used to estimate the dynamic properties of the sensors. A value $\tau_{0.9}$ was estimated as the time required for conductivity signal of the sensor to attain 90% of its equilibrium value after an injection of the hydrogen-air mixture to the measuring chamber of the sensor. The recovery time (τ_{relax}) was estimated as the time required for the conductivity signal of the sensor to attain 10% of its equilibrium value in the hydrogen-air mixture after applying clean air to the measuring chamber.

3. Results and Discussion

Study by the DTA-DTG method of the thermal decomposition process of the obtained xerogel (Figure 1) showed that a weight loss occurs in several steps. The first step (up to 100°C) corresponds to loss of physically sorbed water (~10 wt.%) with endoeffect at 43°C on the DTA curve. Further increase in the temperature up to 600°C leads to a weight loss (~8 wt.%) corresponding to the removal of the strongly bounded water. It should be noted that in this temperature range, partial crystallization of the tin dioxide can also occur and a presence of a broadened peak of exoeffect on the DTA curve (Figure 1) could indicate this process.

Several absorption bands can be observed in the IR spectra of the xerogel and the materials obtained by its temperature treatment up to 400°C with isothermal exposure at this temperature during 1 hour 20 minutes and 2 hours 20 minutes: the absorption band at 1632 cm^{-1} that refers to deformation vibrations of the adsorbed water, a wide absorption band in the region at 3000–3600 cm^{-1} corresponding to the total contribution of stretching vibrations of surface hydroxyl groups and the water adsorbed on the surface, and two intense absorption bands in the region at 550–600 cm^{-1} and 650–680 cm^{-1} corresponding to vibrations of the bond between tin atoms and oxygen for the terminal and bridge fragments, respectively [23, 24]. In the last case, the absorption band at 660 cm^{-1} is the characteristic for the O-Sn-O fragment [24]. It should be noted that an increase in the duration of the temperature treatment of the xerogel from 1 hour 20 minutes to 2 hours 20 minutes

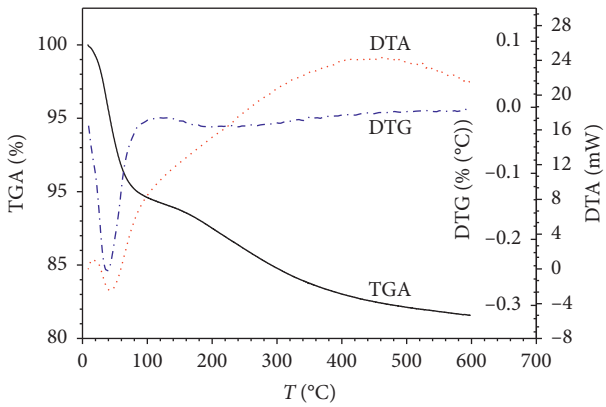

Figure 1: Thermal analysis data for xerogel.

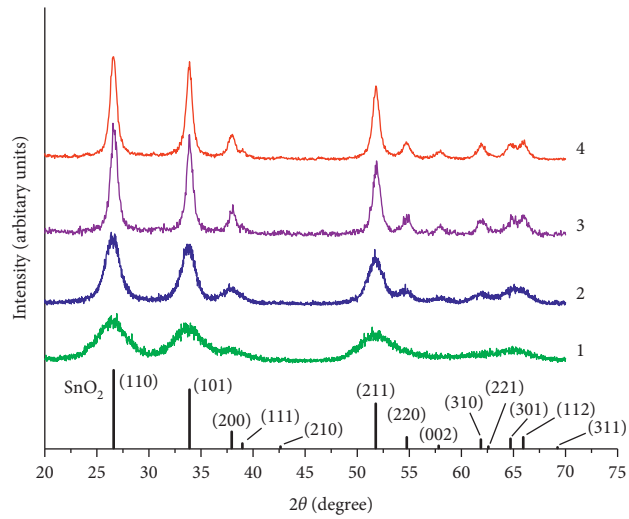

Figure 2: XRD data for xerogel (1); material obtained through temperature treatment of xerogel at 400°C during 2 hours 20 minutes (2); undoped sensor material (3); sensor material doped with 0.24 wt.% Pd (4).

leads to a slight shift (5 cm^{-1}) of the absorption band at 650–680 cm^{-1} to the larger wave numbers region. In these conditions, the absorption band at 590 cm^{-1} for the xerogel shifts to 616 cm^{-1} and to 631 cm^{-1} after 1 hour 20 minutes and 2 hour 20 minutes at 400°C, respectively, due to the formation of the crystalline structure of the nanomaterial [24, 25].

Additional formation of the SnO_2 structure accompanied with rearrangement of tin and oxygen atoms after the temperature treatment of the xerogel is also evidenced by a change in the ratio between the intensity of the absorption bands corresponded to the terminal Sn-O groups and to the bridge fragments. Higher band intensity of the terminal fragments in comparison with the bridge ones in the material heated at 400°C for 2 hours 20 minutes may be attributed to the formation of the SnO_2 crystal structure as it was observed for the materials obtained in [25].

According to the XRD analysis (Figure 2), the diffraction patterns of the xerogel and the materials obtained after xerogel thermal treatment at the temperature range of 400–600°C are broadened that indicates the nanoscale nature of the samples regardless of their isothermal processing time (1 hour 20 min and 2 hours 20 min) at different temperatures (Table 1). It was established that all obtained materials have the cassiterite structure (ICDD PDF-2 Version 2.0602 (2006), card no. 00-041-1445). Calculated lattice parameters are listed in Table 1. Estimation of the materials XRD particle sizes using the Scherrer equation has shown that the SnO_2 particle sizes increase from 4.8 to 12.1 nm (Table 1) with an increase in the isothermal processing temperature of the xerogel. Such increase should lead to a decrease in the specific surface area (S_{sp}) of the material that was experimentally observed: the value of S_{sp} decreased from 110 to 37 m^2/g when isothermal processing temperature increased from 400 to 600°C (Table 1).

It should be noted that changes in isothermal processing time do not make any significant influence on the specific surface area: the value of S_{sp} decreases from 85 to 81 m^2/g at 450°C and from 60 to 58 m^2/g at 500°C when the processing time increases from 1 hour 20 minutes to 2 hour 20 minutes, respectively. Thus, it can be assumed that exposure temperature makes a greater impact on the particles sizes than the processing time. For the samples obtained through the temperature treatment of the xerogel at 400°C during 1 hour 20 minutes, the specific surface area was not measured because the preparation of the sample required high-temperature degasation in the argon flow (the temperature range 300–350°C) that can make changes in the incompletely formed crystal structure of this material. Thus, the obtained value of the specific surface area will not be objective and representative.

The TEM study of the material obtained by the xerogel thermal treatment at 400°C for 2 hours 20 minutes showed that it consisted of individual nanoparticles with sizes from 3 to 9 nm (average size of the nanoparticles is 5–6 nm) (Figure 3(a)). The presence of the nanosized crystalline particles for this material is confirmed by the ring-shaped electron diffraction pattern presented in the inset of Figure 3(a). The specific surface area of the synthesized nanosized tin dioxide is 110 m^2/g (Table 1).

Thus, the thermal treatment of the xerogel up to 400°C during 2 hours 20 minutes is sufficient to provide formation of the nanoscale crystalline SnO_2 with an average particle size 5–6 nm. This material was chosen as the initial for creating the adsorption semiconductor sensors. To increase their sensitivity to hydrogen, a small amount of palladium (0.24 wt.%) was added into the gas-sensitive layer. Both types of the obtained gas-sensitive materials (undoped and doped with 0.24 wt.% Pd) consist of the nanosized particles observed by TEM (Figures 3(b) and 3(c)). According to the XRD study, only cassiterite phase was present in the gas-sensitive material (Figure 2). The XRD sizes of SnO_2 particles are 13.9 and 12.6 nm for the undoped and doped with 0.24 wt.% Pd materials, respectively, that could be explained by a stabilization role of the palladium additives [26].

As can be seen in Figure 4, the palladium additive increases the conductivities of the sensors that can be attributed to the increase in the number of defects in the tin dioxide crystal structure that were formed during the

Table 1: Particle sizes of SnO_2 calculated by using the Scherrer equation, lattice parameters, and specific surface areas of the nanomaterials obtained through thermal treatment of the xerogel.

Sample	Nanomaterial formation conditions		XRD size (nm)	S_{sp} (m^2/g)	Lattice parameters	
	T (°C)	Isothermal processing time			a (Å)	c (Å)
Xerogel	90	24 h	~3		4.77 ± 0.03	3.171 ± 0.06
SnO_2	400	1 h 20 min	4.8		4.732 ± 0.005	3.190 ± 0.005
SnO_2	400	2 h 20 min	5.3	110	4.739 ± 0.005	3.180 ± 0.005
SnO_2	450	1 h 20 min	6.5	85	4.749 ± 0.005	3.191 ± 0.005
SnO_2	500	1 h 20 min	8.3	60	4.745 ± 0.005	3.189 ± 0.005
SnO_2	550	1 h 20 min	9.9	48	4.743 ± 0.005	3.185 ± 0.005
SnO_2	600	1 h 20 min	12.1	37	4.72 ± 0.005	3.190 ± 0.005

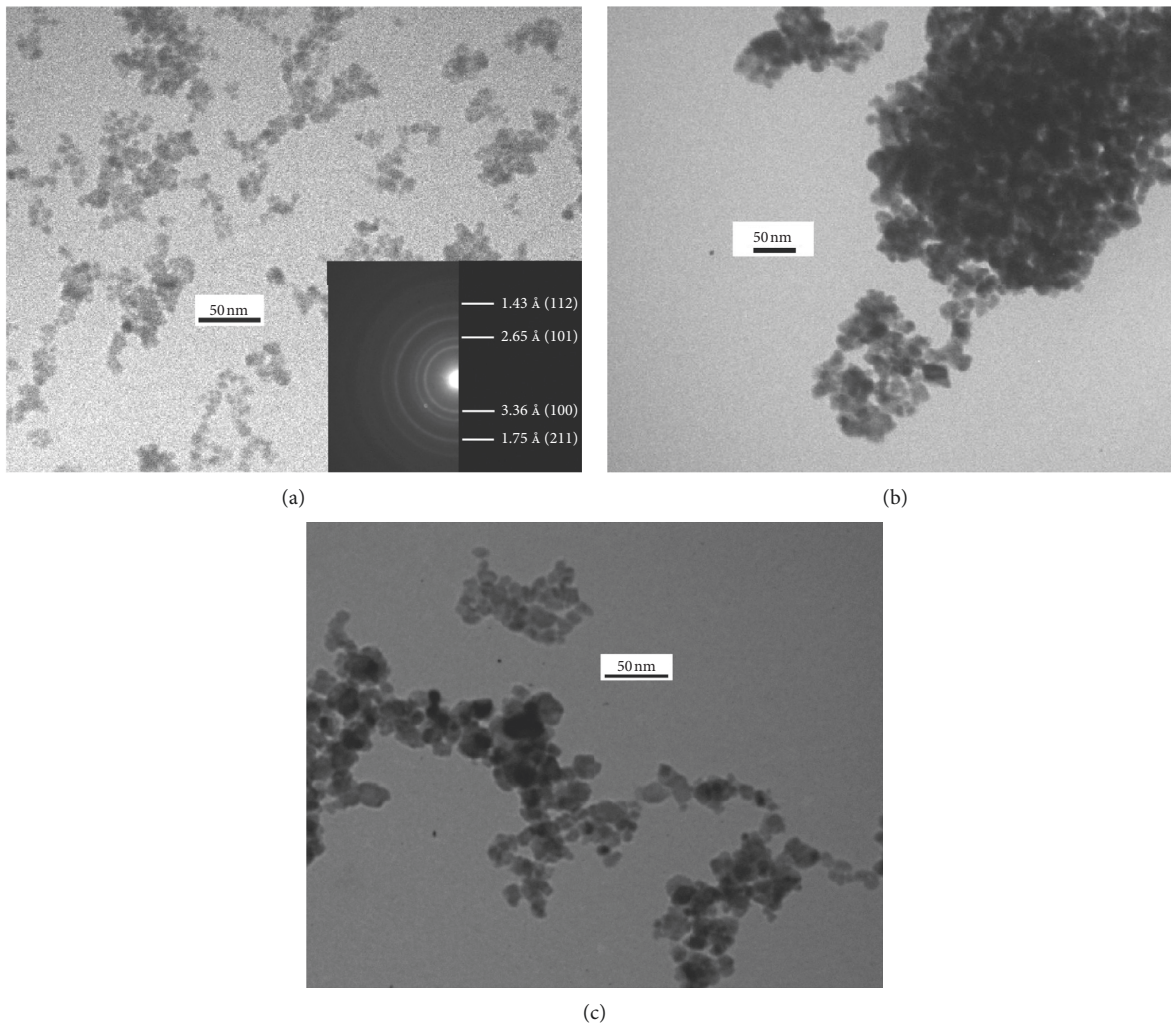

Figure 3: TEM image of the (a) material obtained through calcination of the xerogel at 400°C during 2 hour 20 minutes (electron diffraction with d-spacing and corresponding *hkl* indices for SnO_2 (in round brackets) is presented in the inset), (b) undoped, and (c) doped with 0.24 wt.% Pd gas-sensitive materials on the base of nanosized SnO_2.

high-temperature sensor treatment process due to the introduction of palladium [27]. It should be noted that both types of the sensors (based on unmodified SnO_2 and Pd/SnO_2) demonstrate extreme dependences of the gas-sensitive layer conductivities on the operational temperature of the sensor. Such character of the conductivity changes can be caused by the influence of oxygen adsorption-desorption processes occurring on the sensor surface. An increase in the operational temperature of the sensors from 225 to 290°C (for the sensors based on Pd/SnO_2) and up to 325–345°C (for the sensors based on unmodified SnO_2) can lead to an increase in the amount of the chemisorbed oxygen that, in turn, leads to a decrease in the sensors conductivities [13, 14]. A following increase

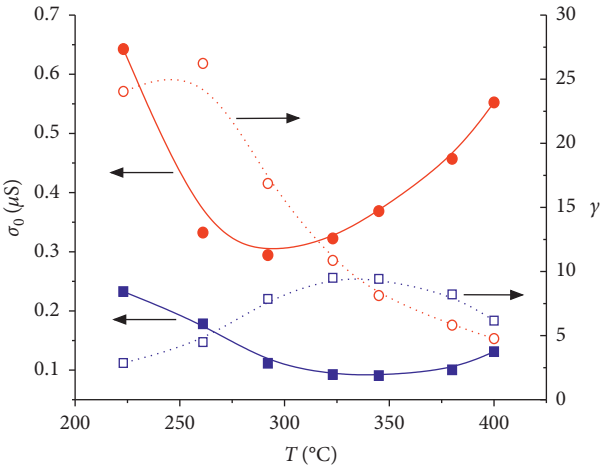

FIGURE 4: Dependencies of conductivity in air (σ_0) and response to hydrogen (γ) of the sensors based on undoped SnO_2 (squares connected by blue lines) and Pd/SnO_2 (circuits connected by red lines) on the sensor operational temperature.

in the operational temperature of the sensor can facilitate the desorption of the chemisorbed oxygen and, thus, leads to an increase in the sensor conductivity (Figure 4).

As can be seen from Figure 4, the sensors based on the unmodified SnO_2 have the highest response value to 44 ppm H_2 (ca. 9.4–9.5) at the same temperature range where the minimal conductivities of the sensors were observed (325–345°C, Figure 4). Such behavior of the sensor parameter changes allowed to conclude that the formation of the sensor responses is greatly influenced by the amount of the chemisorbed oxygen available for the hydrogen oxidation. For the sensors based on the Pd/SnO_2 material, the highest sensor responses to 44 ppm H_2 are observed at 260°C, and it is equal to ~26 which is much higher than the responses to H_2 of the sensors without any additives (Figure 4). The discrepancy between the maximum of the γ dependence on temperature (260°C) and the minimum of the σ_0 dependence on temperature (290°C) can be explained by the significant catalytic activity of palladium in the hydrogen oxidation reaction [17]. Above 260°C, the hydrogen oxidation rate on the palladium can be high enough to provide the formation of reaction products in a large amount. The products prevent or complicate the consumption of the oxygen chemisorbed on the tin dioxide surface by the hydrogen oxidation reaction that occurred on palladium, and thus, such "blocking" of the sensor surface could reduce the sensor responses to hydrogen [13, 14]. The assumption of SnO_2 surface blocking by the hydrogen oxidation products and the oxygen desorption correlates well with a further decrease in the sensitivities of the Pd/SnO_2-based sensors with an increase in their operational temperature. It can be seen (Figure 4) that the sensor responses in the operational temperature range of 345–400°C become even less than the responses of the sensors based on the unmodified SnO_2 probably due to almost complete isolation of the tin dioxide surface from hydrogen by increasing the amount of the reaction products formed on the palladium particles.

To assess the potential usage of the Pd/SnO_2-based sensors for hydrogen detection in air, the dependences of conductivity changes on time with the change of analyzed gas mixtures surrounding the sensors were studied at the different operational temperatures of the sensors (Figure 5). It was found that in the operational temperature range of 260–400°C, the sensors possess good dynamic properties: a steady-state conductivity level in the presence of 44 ppm H_2 and in clean air is attained quickly. In particular, values $\tau_{0,9}$ are in the range of 8–29 s and τ_{relax} falls in the range 12–28 s depending on the operational temperature of the sensor (Table 2).

As can be seen in Figure 5, the time required to achieve the steady-state conductivity level in the presence of 44 ppm H_2 at the sensor operational temperature 225°C is ca. 7 minutes that is significantly bigger in comparison with the higher operational temperatures. Further increase in the operational temperature will lead to an improvement of the sensor dynamic properties, since the rates of the chemical reactions (oxygen chemisorption and catalytic reaction of hydrogen oxidation), the diffusion of the reagents into the gas-sensitive layer, and the rates of the reaction products elimination from the sensor surface increase significantly at the higher sensor temperatures. This statement is in good correspondence with observed experimental data (Figure 5 and Table 2). It is clear from Table 2 that the values of $\tau_{0,9}$ and τ_{relax} decrease with the increase in the operational temperature of the sensor. Obtained values are better than those previously reported in the literature (where $\tau_{0,9} = 2$ min and $\tau_{relax} = 15$ min at 300°C) [28]. Thus, the comparison of the sensor responses data with their dynamic properties allowed to determine the optimal operational temperature for the 0.24 wt.% Pd/SnO_2-based sensors (about 260°C).

To determine a range of the hydrogen detection in air for the Pd/SnO_2-based sensor, the dependences of changes in the sensor conductivities on the hydrogen content in air ambient were studied in the concentration interval 3–935 ppm H_2 at the optimal sensor operational temperature (260°C) (Figure 6). It can be seen that the studied sensor can measure hydrogen in the wide range of its concentration: the response values of the sensors were found to be 5.7 and 193 for 3 and 935 ppm H_2 in air ambient, respectively. Besides, the conductivity level of the sensor in the presence of 3 ppm H_2 demonstrates good repeatability (inset in Figure 6). There are no evidences of a memory effect of the sensor and distortion of the conductivity value in 3 ppm H_2 by influence of 935 ppm H_2 applied to the sensor previously. Thus, the sensors based on Pd/SnO_2 can be used for the reliable detection of hydrogen in air ambient.

The dependence of the conductivity of the sensor based on Pd/SnO_2 on the hydrogen content in air is shown in Figure 7. As it can be seen, in linear scale, σ_g increases with increasing the H_2 content in air over all the measured hydrogen concentration ranges. In logarithmic scale, the dependence is linear and its slope is equal to 0.62:

$$\ln(\sigma_g) = -13.83 + 0.62 \cdot \ln(C_{H_2}). \quad (2)$$

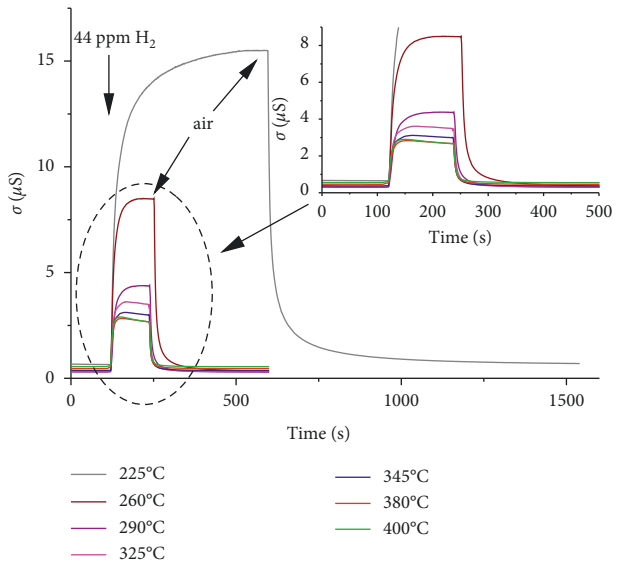

Figure 5: Change in conductivity in time for the 0.24 wt.% Pd/SnO_2-based sensor at different operational temperatures when gas mixture surrounding the sensor was subsequently changed from air to 44 ppm H_2 in air ambient and from 44 ppm H_2 to air.

Table 2: Response ($\tau_{0,9}$) and recovery (τ_{relax}) times to 44 ppm H_2 in air ambient for the 0.24 wt.% Pd/SnO_2-based sensor at its different operational temperatures.

T (°C)	225	260	290	325	345	380	400
$\tau_{0,9}$ (s)	128	29	23	15	12	10	8
τ_{relax} (s)	78	28	23	21	15	13	12

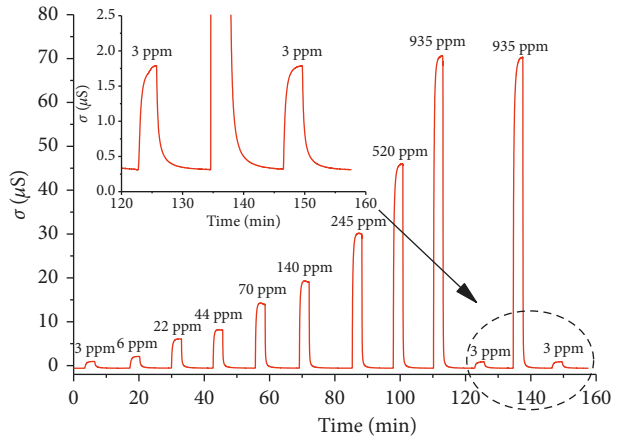

Figure 6: Change in conductivity for the 0.24 wt.% Pd/SnO_2-based sensor versus stepwise change of hydrogen concentration in gas mixture surrounding the sensors at sensor temperature 260°C.

The obtained value for the slope is in good correspondence with the reported data for the typical slope of the conductivity dependence on the concentration of the reducing gases for the adsorption semiconductor sensors in the logarithmic scale [29]. The ability to linearize well the dependence in the logarithmic scale makes a periodic calibration of the sensor during its operation easier because it can be performed using at least two points of H_2 concentrations only.

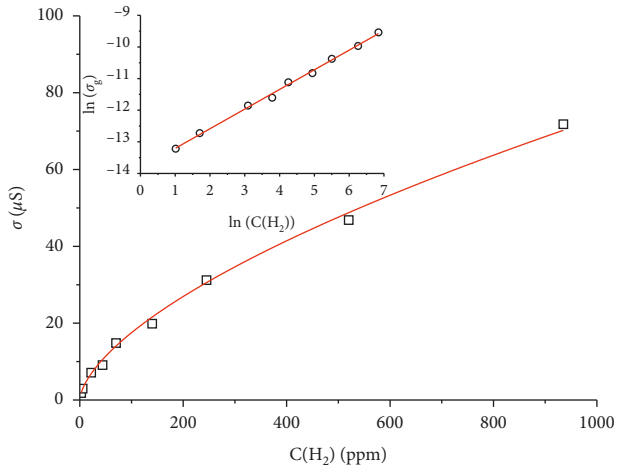

Figure 7: Dependence of conductivity for 0.24 wt.% Pd/SnO_2-based sensor versus H_2 concentration in air ambient in linear and logarithmic scales (inset).

4. Conclusions

Nanosized tin dioxide material with an average particle size of 5.3 nm allowed to create Pd-doped gas-sensitive material for highly sensitive hydrogen sensors. The optimal sensors based on Pd/SnO_2 nanomaterial possess a high response to microconcentration of H_2 (44 ppm in air ambient), a wide range of hydrogen detection in air (3–935 ppm H_2), good stability, lack of the sensor memory effect after exposure to a high hydrogen concentration, and good dynamic properties. These properties make the studied sensors promising for further application in creation of gas analytical devices intended to detect H_2 in air ambient.

Data Availability

The data used to support the findings of this study are included within the article.

Conflicts of Interest

The authors declare that they have no conflicts of interest.

References

[1] S. Basu and A. Dutta, "Room-temperature hydrogen sensors based on ZnO," *Materials Chemistry and Physics*, vol. 47, no. 1, pp. 93–96, 1997.

[2] I. S. Mulla, S. D. Pradhan, and K. Vijayamohanan, "Humidity-sensing behaviour of surface-modified zirconia," *Sensors and Actuators A: Physical*, vol. 57, no. 3, pp. 217–221, 1996.

[3] V. Guidi, M. C. Carotta, M. Ferroni, G. Martinelli, and M. Sacerdoti, "Effect of dopants on grain coalescence and oxygen mobility in nanostructured titania anatase and rutile," *The Journal of Physical Chemistry B*, vol. 107, no. 1, pp. 120–124, 2003.

[4] A. A. Tomchenko, V. V. Khatko, and I. L. Emelianov, "WO_3 thick-film gas sensors," *Sensors and Actuators B: Chemical*, vol. 46, no. 1, pp. 8–14, 1998.

[5] G. Kelp, T. Tätte, S. Pikker et al., "Self-assembled SnO_2 micro- and nanosphere-based gas sensor thick films from an alkoxide-derived high purity aqueous colloid precursor," *Nanoscale*, vol. 8, no. 13, pp. 7056–7067, 2016.

[6] M. Batzill and U. Diebold, "The surface and materials science of tin oxide," *Progress in Surface Science*, vol. 79, no. 2–4, pp. 47–154, 2005.

[7] G. De, A. Licciulli, C. Massaro et al., "Sol-gel derived pure and palladium activated tin oxide films for gas-sensing applications," *Sensors and Actuators B: Chemical*, vol. 55, no. 2-3, pp. 134–139, 1999.

[8] J. C. Kim, H. K. Jun, J.-S. Huh, and D. D. Lee, "Tin oxide-based methane gas sensor promoted by alumina-supported Pd catalyst," *Sensors and Actuators B: Chemical*, vol. 45, no. 3, pp. 271–277, 1997.

[9] A. Cabot, J. Arbiol, J. R. Morante, U. Weimar, N. Bârsan, and W. Göpel, "Analysis of the noble metal catalytic additives introduced by impregnation of as obtained SnO_2 sol-gel nanocrystals for gas sensors," *Sensors and Actuators B: Chemical*, vol. 70, no. 1–3, pp. 87–100, 2000.

[10] F. Pourfayaz, Y. Mortazavi, A. Khodadadi, and S. Ajami, "Ceria-doped SnO_2 sensor highly selective to ethanol in humid air," *Sensors and Actuators B: Chemical*, vol. 130, no. 2, pp. 625–629, 2008.

[11] A. V. Marikutsa, M. N. Rumyantseva, A. M. Gaskov, and A. M. Samoylov, "Nanocrystalline tin dioxide: basics in relation with gas sensing phenomena. Part I. physical and chemical properties and sensor signal formation," *Inorganic Materials*, vol. 51, no. 13, pp. 1329–1347, 2015.

[12] E. Roduner, "Size matters: why nanomaterials are different," *Chemical Society Reviews*, vol. 35, no. 7, pp. 583–592, 2006.

[13] T. A. Miller, S. D. Bakrania, C. Perez, and M. S. Wooldridge, "Nanostructured tin dioxide materials for gas sensor applications," in *Functional Nanomaterials*, K. E. Geckeler and E. Rosenberg, Eds., p. 515, American Scientific Publishers, Valencia, Spain, 2006.

[14] N. Yamazoe and K. Shimanoe, "New perspectives of gas sensor technology," *Sensors and Actuators B: Chemical*, vol. 138, no. 1, pp. 100–107, 2009.

[15] A. Gurlo, "Nanosensors: towards morphological control of gas sensing activity. SnO_2, In_2O_3, ZnO and WO_3 case studies," *Nanoscale*, vol. 3, no. 1, pp. 154–165, 2011.

[16] C. Xu, J. Tamaki, N. Miura, and N. Yamazoe, "Grain size effects on gas sensitivity of porous SnO_2-based elements," *Sensors and Actuators B: Chemical*, vol. 3, no. 2, pp. 147–155, 1991.

[17] N. Yamazoe, Y. Kurokawa, and T. Seiyama, "Effects of additives on semiconductor gas sensors," *Sensors and Actuators*, vol. 4, pp. 283–289, 1983.

[18] R. Alcántara, F. F. Madrigal, P. Lavela, C. Pérez-Vicente, and J. Tirado, "Tin oxalate as a precursor of tin dioxide and electrode materials for lithium-ion batteries," *Journal of Solid State Electrochemistry*, vol. 6, no. 1, pp. 55–62, 2001.

[19] L. P. Oleksenko, G. V. Fedorenko, and N. P. Maksymovych, "Platinum-containing adsorption-semiconductor sensors based on nanosized tin dioxide for methane detection," *Theoretical and Experimental Chemistry*, vol. 53, no. 4, pp. 259–264, 2017.

[20] C. Hammond, *The Basics of Crystallography and Diffraction*, Oxford University Press, Oxford, UK, 2009.

[21] V. Vorotyntsev, N. Maksimovich, L. Yeremina, O. Kaskevich, and N. Nikitina, "Adsorption semiconductor gas sensors and heterogeneous catalytic reaction mechanisms," *Sensors and Actuators B: Chemical*, vol. 36, no. 1–3, pp. 333–337, 1996.

[22] G. V. Fedorenko, L. P. Oleksenko, N. P. Maksymovych, and I. P. Matushko, "Semiconductor adsorption sensors based on nanosized Pt/SnO_2 materials and their sensitivity to methane," *Russian Journal of Physical Chemistry A*, vol. 89, no. 12, pp. 2259–2262, 2015.

[23] G. Zhang and M. Liu, "Preparation of nanostructured tin oxide using a sol-gel process based on tin tetrachloride and ethylene glycol," *Journal of Materials Science*, vol. 34, no. 13, pp. 3213–3219, 1999.

[24] J. C. Giuntini, W. Granier, J. V. Zanchetta, and A. Taha, "Sol-gel preparation and transport properties of a tin oxide," *Journal of Materials Science Letters*, vol. 9, no. 12, pp. 1383–1388, 1990.

[25] B. Orel, U. Lavrenčič-Štankgar, Z. Crnjak-Orel, P. Bukovec, and M. Kosec, "Structural and FTIR spectroscopic studies of gel-xerogel-oxide transitions of SnO_2 and SnO_2: Sb powders and dip-coated films prepared via inorganic sol-gel route," *Journal of Non-Crystalline Solids*, vol. 167, no. 3, pp. 272–288, 1994.

[26] G. Fedorenko, L. Oleksenko, N. Maksymovych, G. Skolyar, and O. Ripko, "Semiconductor gas sensors based on Pd/SnO_2 nanomaterials for methane detection in air," *Nanoscale Research Letters*, vol. 12, no. 1, p. 329, 2017.

[27] K. Chatterjee, S. Chatterjee, A. Banerjee et al., "The effect of palladium incorporation on methane sensitivity of antimony doped tin dioxide," *Materials Chemistry and Physics*, vol. 81, no. 1, pp. 33–38, 2003.

[28] Y. C. Lee, H. Huang, O. K. Tan, and M. S. Tse, "Semiconductor gas sensor based on Pd-doped SnO_2 nanorod thin films," *Sensors and Actuators B: Chemical*, vol. 132, no. 1, pp. 239–242, 2008.

[29] N. Yamazoe and K. Shimanoe, "Theory of power laws for semiconductor gas sensors," *Sensors and Actuators B: Chemical*, vol. 128, no. 2, pp. 566–573, 2008.